

Crystal Structure and Cation Transport Properties of the Layered Monodiphosphates: $\text{Li}_9\text{M}_3(\text{P}_2\text{O}_7)_3(\text{PO}_4)_2$ ($M = \text{Al, Ga, Cr, Fe}$)

S. Poisson,^{*,1} F. d'Yvoire,^{*} N. Nguyen-Huy-Dung,[†] E. Bretey,^{*} and P. Berthet^{*}

^{*}Laboratoire de Chimie des Solides, URA-CNRS 446, Bât. 414, Université Paris-Sud, 91405 Orsay Cedex, France; and

[†]Laboratoire de Cristallographie Bioinorganique, Faculté des Sciences Pharmaceutiques et Biologiques, 5 rue J.B. Clément, 92296 Châtenay-Malabry Cedex, France

Received September 4, 1997; in revised form December 31, 1997; accepted January 11, 1998

A new series of isotopic monodiphosphates of general formula $\text{Li}_9\text{M}_3(\text{P}_2\text{O}_7)_3(\text{PO}_4)_2$ with $M = \text{Al, Ga, Cr, Fe}$ was synthesized by flux methods. The crystal structure of the aluminum and iron members is described here. They crystallize in the trigonal space group $P3c1$ with $a = 9.553(1)$, $c = 13.492(2)$ Å ($M = \text{Al}$), $a = 9.726(1)$, $c = 13.615(2)$ Å ($M = \text{Fe}$) and $Z = 2$. The structure consists of ${}_{\infty}^2[(\text{MP}_2\text{O}_7)_3(\text{PO}_4)_2]^{9-}$ corrugated layers, parallel to (001), separated by lithium ions. The layers are built up of MO_6 octahedra sharing corners with PO_4 tetrahedra and P_2O_7 groups. Three nonequivalent lithium ions are present according to the structural formula $\text{Li}(1)_1\text{Li}(2)_2\text{Li}(3)_6[\text{MP}(2)_2\text{O}_7]_3[\text{P}(1)\text{O}_4]_2$. The crystals exhibit a lithium ion conduction mainly parallel to (001) but with rather low conductivity values: $\sigma_{//(001)} = 1.3 \times 10^{-4}$ and $3.0 \times 10^{-6} \Omega^{-1} \text{cm}^{-1}$ at 300°C for $M = \text{Fe}$ and $M = \text{Al}$, respectively. In the presence of acidic aqueous solutions, $\text{Li}_9\text{Fe}_3(\text{P}_2\text{O}_7)_3(\text{PO}_4)_2$ undergoes an ion-exchange reaction between Li^+ and H^+ with the introduction of water molecules, which causes a one-dimensional expansion of the crystals perpendicular to the layers. © 1998 Academic Press

INTRODUCTION

During the past two decades, a number of phosphates belonging to the systems $A_2\text{O}-M_2\text{O}_3-\text{P}_2\text{O}_5$ ($A = \text{Li, Na}$ and $M = \text{Al, Ga, Cr, Fe}$) were shown to exhibit fast A^+ ion transport properties: among them are the Nasicon-type monophosphates $A_3\text{Cr}_2(\text{PO}_4)_3$ and $A_3\text{Fe}_2(\text{PO}_4)_3$ (1–4), the monoclinic $\beta\text{-Fe}_2(\text{SO}_4)_3$ -type modification of $\text{Li}_3\text{Cr}_2(\text{PO}_4)_3$ and $\text{Li}_3\text{Fe}_2(\text{PO}_4)_3$ (2, 5–7), the monodiphosphates $\text{Na}_7(\text{MP}_2\text{O}_7)_4\text{PO}_4$ (8), and the diphosphates $\text{Na}_7\text{M}_3(\text{P}_2\text{O}_7)_4$ (9, 10). All these compounds have a 3D framework made up of corner-sharing MO_6 octahedra and PO_4 tetrahedra, with the A^+ ions located in the interstitial space. Vitreous materials were also prepared in these ternary systems for wide ranges of compositions; many of these glasses present high

Li^+ or Na^+ ion conductivity (11–13). In a recent work devoted to $A_2\text{O}-M_2\text{O}_3-\text{P}_2\text{O}_5$ glasses (14), thermal devitrification studies revealed the existence of a new family of monodiphosphates, $\text{Li}_9\text{M}_3(\text{P}_2\text{O}_7)_3(\text{PO}_4)_2$ ($M = \text{Al, Ga, Cr, Fe}$), characterized by a layered structure. In the present paper, the preparation and crystal data of these compounds are reported. The crystal structure of the Al and Fe members is described as well as their Li^+ ion transport properties.

CHEMICAL SYNTHESSES

The four compounds were prepared by crystallization in a flux of lithium phosphates. Starting materials were Li_3PO_4 , $M_2\text{O}_3$ ($M = \text{Al, Ga, Cr, Fe}$), and $\text{NH}_4\text{H}_2\text{PO}_4$ mixed in molar ratios $\text{Li}/M/\text{P}$: 60/4/36 (55.5/4/40.5 for $M = \text{Al}$). The mixtures were gradually heated up to 900°C in a platinum crucible and cooled at a rate of $50^\circ\text{C}/\text{h}$ down to 850°C , of $2^\circ\text{C}/\text{h}$ between 850 and 600°C and finally of about $200^\circ\text{C}/\text{h}$ down to room temperature.

The X-ray powder diffractograms of the resulting solids revealed the presence of the low-temperature form of $\text{Li}_4\text{P}_2\text{O}_7$ (15) and of the high-temperature form of LiPO_3 (16, 17) together with $\text{Li}_9\text{M}_3(\text{P}_2\text{O}_7)_3(\text{PO}_4)_2$. In order to isolate this new phase, the mixture was treated during 5 days by an aqueous 1 M solution of CH_3COOH which dissolved $\text{Li}_4\text{P}_2\text{O}_7$. A saturated solution of NaCl was then added to the remaining solid to eliminate LiPO_3 through an ion-exchange process similar to that described by Van Wazer for the dissolution of the NaPO_3 long chain polyphosphates (18): the exchange of Li^+ for Na^+ is accompanied by the insertion of water molecules, leading to the formation of a gelatinous matter which can be dissolved in water. The final water-insoluble solid is pure $\text{Li}_9\text{M}_3(\text{P}_2\text{O}_7)_3(\text{PO}_4)_2$.

CRYSTAL DATA AND THERMAL ANALYSIS

The as-prepared compounds are in the form of large plates or hexagonal platelets, with an area up to 1 cm^2 . They

¹ To whom correspondence should be addressed.

TABLE 1
XRPD of $\text{Li}_9\text{M}_3(\text{P}_2\text{O}_7)_3(\text{PO}_4)_2$ ($M = \text{Al}, \text{Ga}, \text{Cr}, \text{Fe}$)

$M = \text{Al}$				$M = \text{Ga}$				$M = \text{Cr}$				$M = \text{Fe}$			
I^a	$d_{\text{obs}}(\text{Å})$	$d_{\text{calc}}(\text{Å})$	$h k l$	I^a	$d_{\text{obs}}(\text{Å})$	$d_{\text{calc}}(\text{Å})$	$h k l$	I^a	$d_{\text{obs}}(\text{Å})$	$d_{\text{calc}}(\text{Å})$	$h k l$	I^a	$d_{\text{obs}}(\text{Å})$	$d_{\text{calc}}(\text{Å})$	$h k l$
w	8.275	8.2734	1 0 0	m	8.35	8.3511	1 0 0	w	8.36	8.3710	1 0 0	w	8.429	8.4230	1 0 0
vst	6.742	6.7460	0 0 2	vst	6.795	6.7960	0 0 2	vst	6.794	6.7940	0 0 2	vst	6.803	6.8074	0 0 2
m	5.227	5.2283	1 0 2	m	5.271	5.2711	1 0 2	m	5.273	5.2752	1 0 2	m	5.295	5.2944	1 0 2
m	4.776	4.7766	1 1 0	m	4.820	4.8215	1 1 0	m	4.829	4.8330	1 1 0	m	4.858	4.8630	1 1 0
m	4.502	4.5028	1 1 1	vw	4.541	4.5441	1 1 1			4.5535	1 1 1	vw	4.577	4.5796	1 1 1
st	4.137	4.1367	2 0 0	vw	4.175	4.1755	2 0 0	w	4.188	4.1855	2 0 0	m	4.2111	4.2115	2 0 0
st	3.899	3.8983	1 1 2	vst	3.931	3.9324	1 1 2	st	3.938	3.9382	1 1 2	st	3.9565	3.9570	1 1 2
vw	3.5264	3.5265	2 0 2	vw	3.557	3.5577	2 0 2	vw	3.562	3.5635	2 0 2	vw	3.5815	3.5815	2 0 2
m	3.3724	3.3730	0 0 4	vw	3.399	3.3980	0 0 4	w	3.397	3.3970	0 0 4	w	3.4040	3.4037	0 0 4
m	3.2745	3.2744	1 1 3	m	3.3025	3.3017	1 1 3	m	3.3050	3.3049	1 1 3	m	3.3184	3.3179	1 1 3
st	3.1272	3.1270	2 1 0	m	3.1547	3.1564	2 1 0	m	3.1638	3.1639	2 1 0	st	3.1832	3.1836	2 1 0
		3.1234	1 0 4	vw	3.1457	3.1474	1 0 4	vw	3.148	3.1477	1 0 4	vw	3.1540	3.1558	1 0 4
vst	3.0462	3.0463	2 1 1	vw	3.073	3.0746	2 1 1	vst	3.0809	3.0815	2 1 1	vst	3.1003	3.1000	2 1 1
m	2.8384	2.8371	2 1 2	w	2.8627	2.8627	2 1 2	vw	2.869	2.8682	2 1 2	vw	2.8841	2.8838	2 1 2
st	2.7583	2.7578	3 0 0	m	2.7835	2.7837	3 0 0	m	2.7909	2.7903	3 0 0	m	2.8069	2.8076	3 0 0
		2.7553	1 1 4	vw	2.778	2.7775	1 1 4			2.7792	1 1 4	vw	2.786	2.7885	1 1 4
vst	2.6139	2.6141	2 0 4	vst	2.6360	2.6356	2 0 4	vst	2.638	2.6376	2 0 4	vst	2.6472	2.6472	2 0 4
st	2.5678	2.5674	2 1 3	st	2.5902	2.5899	2 1 3	m	2.5946	2.5938	2 1 3	st	2.6064	2.6062	2 1 3
m	2.5525	2.5527	3 0 2	w	2.5760	2.5760	3 0 2	vw	2.582	2.5811	3 0 2	w	2.5966	2.5955	3 0 2
m	2.3884	2.3883	2 2 0	m	2.4106	2.4107	2 2 0	w	2.4168	2.4165	2 2 0	w	2.4306	2.4315	2 2 0
w	2.3519	2.3518	2 2 1	w	2.3723	2.3737	2 2 1	vw	2.380	2.3792	2 2 1	vw	2.393	2.3936	2 2 1
		2.3494	1 1 5	w	2.3670	2.3680	1 1 5	vw	2.369	2.3688	1 1 5	vw	2.374	2.3758	1 1 5
w	2.2947	2.2946	3 1 0			2.3162	3 1 0			2.3217	3 1 0	vw	2.335	2.3361	3 1 0
		2.2932	2 1 4	w	2.3120	2.3126	2 1 4			2.3153	2 1 4	vw	2.324	2.3250	2 1 4
vw	2.263	2.2621	3 1 1	st	2.2834	2.2833	3 1 1	w	2.2884	2.2885	3 1 1	w	2.3035	2.3025	3 1 1
		2.2514	2 2 2	vw	2.271	2.2720	2 2 2			2.2768	2 2 2			2.2898	2 2 2
m	2.2489	2.2487	0 0 6	vw	2.265	2.2653	0 0 6	vw	2.265	2.2647	0 0 6	vw	2.269	2.2691	0 0 6
st	2.1722	2.1724	3 1 2	m	2.1928	2.1923	3 1 2	w	2.1969	2.1970	3 1 2	w	2.2094	2.2096	3 1 2
w	2.1700	2.1699	1 0 6	vw	2.186	2.1863	1 0 6	vw	2.186	2.1861	1 0 6	vw	2.190	2.1910	1 0 6
m	2.1352	2.1350	3 0 4	w	2.1544	2.1534	3 0 4	vw	2.157	2.1562	3 0 4	vw	2.165	2.1659	3 0 4
		2.1093	2 2 3	vw	2.127	2.1282	2 2 3			2.1320	2 2 3			2.1433	2 2 3
m	2.0693	2.0683	4 0 0	m	2.0881	2.0878	4 0 0	vw	2.093	2.0927	4 0 0	vw	2.107	2.1057	4 0 0

^a Intensities estimated visually.

are colorless ($M = \text{Al}, \text{Ga}$), light beige ($M = \text{Fe}$) or green ($M = \text{Cr}$). The crystals are optically uniaxial negative.

Weissenberg and precession photographs of Al and Fe crystals showed a trigonal symmetry and led to $P3c1$ and $P\bar{3}c1$ as possible space groups. The isotropy of the four compounds is supported by the close similarity of their X-ray powder diffraction patterns (XRPD), given in Table 1; d_{hkl} values were collected using a Guinier camera with $\text{Al}_4(\text{P}_4\text{O}_{12})_3$ as an internal standard (19). The unit-cell parameters refined from powder data are given in Table 2.

Differential thermal analysis (DTA) experiments performed on the four powdered compounds did not show any structural transition between the room temperature and the incongruent melting temperature (T_m). The solid phases identified in the samples quenched from a temperature T higher than T_m are listed in Table 3.

STRUCTURE OF THE ALUMINUM AND IRON COMPOUNDS

Structure Determination

The crystal of $\text{Li}_9\text{Al}_3(\text{P}_2\text{O}_7)_3(\text{PO}_4)_2$ selected for the X-ray study was an hexagonal plate tabular on (001); the crystal of

TABLE 2
Unit Cell Constants

Compound	a (Å)	c (Å)	V (Å ³)
$\text{Li}_9\text{Al}_3(\text{P}_2\text{O}_7)_3(\text{PO}_4)_2$	9.553(1)	13.492(2)	1066.3(4)
$\text{Li}_9\text{Ga}_3(\text{P}_2\text{O}_7)_3(\text{PO}_4)_2$	9.643(1)	13.592(3)	1094.5(5)
$\text{Li}_9\text{Cr}_3(\text{P}_2\text{O}_7)_3(\text{PO}_4)_2$	9.666(1)	13.588(3)	1099.4(5)
$\text{Li}_9\text{Fe}_3(\text{P}_2\text{O}_7)_3(\text{PO}_4)_2$	9.726(1)	13.615(2)	1115.3(4)

TABLE 3

Melting Temperature (T_m) of Crystalline $\text{Li}_9\text{M}_3(\text{P}_2\text{O}_7)_3(\text{PO}_4)_2$ Determined from DTA Experiments (Heating Rate $10^\circ\text{C}/\text{mn}$) and Solid Phases Present in the Samples after Quenching from $T > T_m$ down to Room Temperature

M	T_m ($^\circ\text{C}$)	T ($^\circ\text{C}$)	Quenched samples
Ga	765	800	GaPO_4 -quartz + glass
Al	790	840	AlPO_4 -tridymite + (?) + glass
Fe	825	860	LiFeP_2O_7 + II- $\text{Li}_3\text{Fe}_2(\text{PO}_4)_3$ (traces) + glass
Cr	1015	1040	LiCrP_2O_7 + II- $\text{Li}_3\text{Cr}_2(\text{PO}_4)_3$ + glass

$\text{Li}_9\text{Fe}_3(\text{P}_2\text{O}_7)_3(\text{PO}_4)_2$ was a trigonal prism limited by $\{110\}$ and $\{001\}$. The centrosymmetric group $P\bar{3}c1$ was found to be correct by structure determination.

TABLE 4

Crystal Data and Experimental Conditions for Crystallographic Analysis of $\text{Li}_9\text{M}_3(\text{P}_2\text{O}_7)_2$ ($M = \text{Al}, \text{Fe}$)

	$M = \text{Al}$	$M = \text{Fe}$
Crystal data		
Crystal system		trigonal
Space group		$P\bar{3}c1$
a (\AA)	9.551(2)	9.721(2)
c (\AA)	13.486(6)	13.594(5)
V (\AA^3)	1065.2(9)	1112.6(9)
Z		2
Formula mass (amu)	855.19	941.78
Crystal size (mm)	$0.25 \times 0.20 \times 0.05$	0.22 along $[001]$ 0.24 along $\langle 110 \rangle$
μ ($\text{MoK}\alpha$) (cm^{-1})	9.050	13.158
D_x (g cm^{-3})	2.666(2)	2.810(2)
Intensity measurement		
Monochromator		graphite
λ ($\text{MoK}\alpha$) (\AA)		0.7107
T (K)		294
Scan mode		ω - 2θ
Scan width (mm)		1.6
Scan speed ($^\circ/\text{min}$)		16.48
θ range ($^\circ$)		2-30
hkl range	$-13 \leq h \leq 13$, $-13 \leq k \leq 13, 0 \leq l \leq 18$	$-13 \leq h \leq 0$, $0 \leq k \leq 13, 0 \leq l \leq 18$
Collected reflections	6194	2432
Observed reflections ($I > 3\sigma(I)$)	3261	1616
Absorption corrections		integration from crystal shape
Transmission factors	min = 0.796 max = 0.956	min = 0.665 max = 0.749
Refinements		
Independent reflections observed		
after averaging ($I > 3\sigma(I)$)	556	770
Number of variables	76	77
$F(000)$	836	457
Refinement method		Full-matrix least-squares on F
Weighting scheme	$w = 1/\sigma(F)^2$	$w = 1$
Agreement factors	$R = 0.022$ $R_w = 0.030$	$R = 0.025$ $R_w = 0.028$
$\Delta\rho_{\text{max}}$ (e \AA^{-3})	0.4(1)	0.5(1)
$\Delta\rho_{\text{min}}$ (e \AA^{-3})	-0.4(1)	-0.5(1)

Intensities were collected at 294 K on a CAD-4 Enraf-Nonius four-circle diffractometer using $\text{MoK}\alpha$ radiation. Crystal data and experimental conditions for intensity measurements and refinements are reported in Table 4; the cell parameters calculated from single-crystal measurements are in good agreement with those refined from powder data (Table 2). Structure determination and refinements were performed using the MolEN program package (20). The intensities were corrected from Lorentz and polarization effects. Absorption corrections were performed using the program ABSCOR (21). Direct methods revealed the coordinates of the phosphorus, aluminum, and iron atoms (22). The other atoms were located by subsequent difference Fourier syntheses. The final atomic parameters are listed in Table 5. Selected distances and angles are listed in Tables 6 and 7.

Description of the Structure

The crystal structure consists of infinite anionic corrugated layers ${}^2_{\infty}[(\text{MP}_2\text{O}_7)_3(\text{PO}_4)_2]^{9-}$, parallel to (001), separated by Li^+ cations, which are distributed over three sites according to the structural formula $\text{Li}(1)_1\text{Li}(2)_2\text{Li}(3)_6(\text{MP}_2\text{O}_7)_3(\text{PO}_4)_2$.

TABLE 5
Atomic Coordinates and Isotropic Thermal Parameters for $\text{Li}_9\text{M}_3(\text{P}_2\text{O}_7)_3(\text{PO}_4)_2$ ($M = \text{Al}, \text{Fe}$)

	Atoms	x	y	z	B_{eq} (\AA^2) ^a
$M = \text{Al}$	P(1)	2/3	1/3	0.62964(8)	0.44(1)
	P(2)	0.31796(7)	0.09144(7)	0.84280(5)	0.47(1)
	Al	0.5659(1)	0	3/4	0.47(2)
	Li(1)	0	0	0	4.2(3)
	Li(2)	2/3	1/3	0.8827(6)	1.5(1)
	Li(3)	0.3380(6)	0.1012(5)	0.0631(4)	1.22(9)
$M = \text{Fe}$	O(1)	2/3	1/3	0.5185(2)	1.71(5)
	O(2)	0.2078(3)	0	3/4	0.72(5)
	O(3)	0.6722(2)	0.1847(2)	0.6682(1)	0.75(3)
	O(4)	0.4809(2)	0.1020(2)	0.8300(1)	0.74(4)
	O(5)	0.3380(2)	0.2594(2)	0.8408(1)	0.66(3)
	O(6)	0.2272(2)	0.0002(2)	0.9337(1)	0.87(4)
	P(1)	2/3	1/3	0.62484(9)	0.47(1)
	P(2)	0.31610(8)	0.08895(8)	0.84424(5)	0.52(1)
	Fe	0.56704(6)	0	3/4	0.52(1)
	Li(1)	0	0	0	5.7(5)
	Li(2)	2/3	1/3	0.8813(7)	1.7(1)
	Li(3)	0.3341(7)	0.0989(6)	0.0631(4)	1.5(1)
O(1)	2/3	1/3	0.5143(3)	2.25(6)	
O(2)	0.2128(3)	0	3/4	0.96(6)	
O(3)	0.6778(2)	0.1899(2)	0.6631(2)	0.92(4)	
O(4)	0.4802(2)	0.1075(2)	0.8324(2)	0.94(4)	
O(5)	0.3297(2)	0.2516(2)	0.8446(1)	0.77(4)	
O(6)	0.2268(3)	-0.0049(2)	0.9330(2)	1.17(4)	

$${}^a B_{\text{eq}} = 4/3 \sum_i \sum_j \mathbf{a}_i \cdot \mathbf{a}_j \cdot \beta_{ij}$$

TABLE 6
Interatomic Distances (Å) and Angle (°) in the Anionic Layers of $\text{Li}_9\text{Al}_3(\text{P}_2\text{O}_7)_3(\text{PO}_4)_2$ and $\text{Li}_9\text{Fe}_3(\text{P}_2\text{O}_7)_3(\text{PO}_4)_2$

$\text{Li}_9\text{Al}_3(\text{P}_2\text{O}_7)_3(\text{PO}_4)_2$						$\text{Li}_9\text{Fe}_3(\text{P}_2\text{O}_7)_3(\text{PO}_4)_2$							
AlO ₆ octahedron						FeO ₆ octahedron							
Al	O(4) ⁱ	O(4)	O(3)	O(3) ⁱ	O(5) ⁱⁱ	O(5) ⁱⁱⁱ	Fe	O(4) ⁱ	O(4)	O(3)	O(3) ⁱ	O(5) ⁱⁱ	O(5) ⁱⁱⁱ
O(4) ⁱ	<i>1.887(2)</i>	2.740(2)	2.770(2)	2.698(2)	3.776(3)	2.603(2)	O(4) ⁱ	<i>1.986(2)</i>	2.881(3)	2.931(3)	2.845(3)	3.974(3)	2.766(3)
O(4)	93.1(1)	<i>1.887(2)</i>	2.698(2)	2.770(2)	2.603(2)	3.776(3)	O(4)	93.0(1)	<i>1.986(2)</i>	2.845(3)	2.931(3)	2.766(3)	3.974(3)
O(3)	94.4(1)	91.2(1)	1.888(2)	3.767(2)	2.744(2)	2.470(3)	O(3)	94.9(1)	91.2(1)	<i>1.995(2)</i>	3.975(2)	2.914(3)	2.572(3)
O(3) ⁱ	91.2(1)	94.4(1)	171.9(1)	<i>1.888(2)</i>	2.470(3)	2.744(2)	O(3) ⁱ	91.2(1)	94.9(1)	171.2(1)	<i>1.995(2)</i>	2.572(3)	2.914(3)
O(5) ⁱⁱ	172.7(1)	86.9(1)	92.9(1)	81.5(1)	<i>1.896(1)</i>	2.773(3)	O(5) ⁱⁱ	171.4(1)	87.9(1)	93.7(1)	80.2(1)	<i>2.000(2)</i>	2.889(3)
O(5) ⁱⁱⁱ	86.9(1)	172.7(1)	81.5(1)	92.9(1)	94.0(1)	<i>1.896(1)</i>	O(5) ⁱⁱⁱ	87.9(1)	171.4(1)	80.2(1)	93.7(1)	92.5(1)	<i>2.000(2)</i>
⟨Al–O⟩: 1.891 Å						⟨Fe–O⟩: 1.993 Å							
P(1)O ₄ tetrahedron					P(1)O ₄ tetrahedron								
P(1)	O(1)	O(3)	O(3) ⁱⁱ	O(3) ^{iv}	P(1)	O(1)	O(3)	O(3) ⁱⁱ	O(3) ^{iv}				
O(1)	<i>1.499(3)</i>	2.485(3)	2.485(3)	2.485(3)	O(1)	<i>1.503(4)</i>	2.489(4)	2.489(4)	2.489(4)				
O(3)	109.8(1)	<i>1.538(2)</i>	2.506(3)	2.506(3)	O(3)	109.7(1)	<i>1.541(2)</i>	2.513(3)	2.513(3)				
O(3) ⁱⁱ	109.8(1)	109.2(1)	<i>1.538(2)</i>	2.506(3)	O(3) ⁱⁱ	109.7(1)	109.2(1)	<i>1.541(2)</i>	2.513(3)				
O(3) ^{iv}	109.8(1)	109.2(1)	109.2(1)	<i>1.538(2)</i>	O(3) ^{iv}	109.7(1)	109.2(1)	109.2(1)	<i>1.541(2)</i>				
P(2)O ₄ tetrahedron in P ₂ O ₇ group					P(2)O ₄ tetrahedron in P ₂ O ₇ group								
P(2)	O(6)	O(5)	O(4)	O(2)	P(2)	O(6)	O(5)	O(4)	O(2)				
O(6)	<i>1.503(2)</i>	2.490(3)	2.533(3)	2.485(2)	O(6)	<i>1.500(2)</i>	2.484(3)	2.538(3)	2.494(2)				
O(5)	111.0(1)	<i>1.517(2)</i>	2.489(3)	2.470(1)	O(5)	110.7(1)	<i>1.520(2)</i>	2.485(4)	2.480(2)				
O(4)	114.0(1)	110.1(1)	<i>1.518(2)</i>	2.525(3)	O(4)	114.3(1)	109.6(1)	<i>1.521(2)</i>	2.528(3)				
O(2)	107.0(1)	105.4(1)	108.8(1)	<i>1.587(1)</i>	O(2)	107.5(1)	105.8(1)	108.6(1)	<i>1.591(1)</i>				
P ₂ O ₇ group: P(2)–O(2)–P(2): 134.3(2)° P(2)–P(2): 2.924(1) Å					P ₂ O ₇ group: P(2)–O(2)–P(2): 137.8(2)° P(2)–P(2): 2.968(1) Å								

Note. The *M*–O or P–O distances are shown in italics. The O–*M*–O or O–P–O angles are given below the diagonal and the O–O distances are given above.

Symmetry code: (i) $x - y, -y, 3/2 - z$; (ii) $1 - y, x - y, z$; (iii) $1 - x, y - x, 3/2 - z$; (iv) $1 - x + y, 1 - x, z$.

Anionic layers. The anionic layers are of two types which are symmetrically equivalent by inversion and alternate along *c*. They are composed of *MO*₆ octahedra sharing corners with monophosphate tetrahedra P(1)O₄ and diphosphate groups P(2)₂O₇ (Fig. 1).

The *MO*₆ octahedron exhibits a two-fold internal symmetry. It shares two adjacent oxygen atoms O(4) with a diphosphate group (Fig. 2). In other words, *M* is chelated by a P₂O₇ group as observed in many *M*^I *M*^{III} diphosphates such as LiFeP₂O₇ (23), NaFeP₂O₇-II (24), KAlP₂O₇ (25), or Na₇Fe₃(P₂O₇)₄ (9). The *MO*₆ octahedron is also linked to two other P₂O₇ groups, each connection being ensured by a single oxygen atom (O(5)). Each of the two remaining oxygens of the *MO*₆ octahedron, (O(3)), is shared with a monophosphate tetrahedron. The Al–O and Fe–O average distances are close to those observed in KAlP₂O₇ (25) and LiFeP₂O₇ (23), respectively.

The diphosphate P(2)₂O₇ unit also adopts a binary internal symmetry with the bridging oxygen O(2) located onto a two-fold axis. It shares two symmetrical equivalent oxy-

gen atoms O(4) with one *MO*₆ octahedron; moreover, each P(2)O₄ tetrahedron is linked to another octahedron via O(5). The P(2)O₃ terminal groups are in a nearly eclipsed configuration with a dihedral angle between the O(4)–P(2)–P'(2) and O'(4)–P'(2)–P(2) planes of 12.4(2)° (*M* = Al) and 16.3(2)° (*M* = Fe). As a comparison, the corresponding values in Na₇(FeP₂O₇)₄PO₄ (8, 27), LiFeP₂O₇ (23), and NaFeP₂O₇-II (24) are 13.4°, 8.9°, and about 12°, respectively, whereas the P₂O₇ configuration is staggered in KAlP₂O₇ (25).

Like in many diphosphates (28), the longest P–O distance in the P₂O₇ unit corresponds to the bridging oxygen O(2), while the shortest one involves the terminal oxygen atom O(6), which is not shared with a *MO*₆ octahedron; O(6) lies in the immediate environment of Li(1) and Li(3) and shows a relatively high thermal parameter (see Table 5).

The P(1)O₄ tetrahedron (internal symmetry *3m*) presents two types of oxygen atoms, O(1) and O(3). O(1) is located on the ternary axis and lies in the environment of Li(2) while each oxygen atom O(3) is shared with a *MO*₆ octahedron.

TABLE 7
Interatomic Distances (Å) and Angles (°) in the LiO_n Polyhedra of $\text{Li}_9\text{M}_3(\text{P}_2\text{O}_7)_3(\text{PO}_4)_2$

$M = \text{Al}$							$M = \text{Fe}$						
Li(1)O₆ trigonal antiprism							Li(1)O₆ trigonal antiprism						
Li(1)	O(6) ^v	O(6) ^{vi}	O(6) ^{vii}	O(6) ^{viii}	O(6) ^{ix}	O(6) ^x	Li(1)	O(6) ^v	O(6) ^{vi}	O(6) ^{vii}	O(6) ^{viii}	O(6) ^{ix}	O(6) ^x
O(6) ^v	<i>2.346(2)</i>	4.692(3)	3.757(3)	2.810(3)	3.756(3)	2.810(3)	O(6) ^v	<i>2.408(3)</i>	4.816(3)	3.861(3)	2.878(3)	3.861(3)	2.878(3)
O(6) ^{vi}	180.0	<i>2.346(2)</i>	2.810(3)	3.757(3)	2.810(3)	3.756(3)	O(6) ^{vi}	180.0	<i>2.408(3)</i>	2.878(3)	3.861(3)	2.878(3)	3.861(3)
O(6) ^{vii}	106.4(1)	73.6(1)	<i>2.346(2)</i>	4.692(3)	3.756(3)	2.810(3)	O(6) ^{vii}	106.6(1)	73.4(1)	<i>2.408(3)</i>	4.816(3)	3.861(3)	2.878(3)
O(6) ^{viii}	73.6(1)	106.4(1)	180.0	<i>2.346(2)</i>	2.810(3)	3.756(3)	O(6) ^{viii}	73.4(1)	106.6(1)	180.0	<i>2.408(3)</i>	2.878(3)	3.861(3)
O(6) ^{ix}	106.4(1)	73.6(1)	106.4(1)	73.6(1)	<i>2.346(2)</i>	4.692(3)	O(6) ^{ix}	106.6(1)	73.4(1)	106.6(1)	73.4(1)	<i>2.408(3)</i>	4.816(3)
O(6) ^x	73.6(1)	106.4(1)	73.6(1)	106.4(1)	180.0	<i>2.346(2)</i>	O(6) ^x	73.4(1)	106.6(1)	73.4(1)	106.6(1)	180.0	<i>2.408(3)</i>
Li(2)O₄ tetrahedron							Li(2)O₄ tetrahedron						
Li(2)	O(1) ^{xi}	O(4)	O(4) ⁱⁱ	O(4) ^{iv}			Li(2)	O(1) ^{xi}	O(4)	O(4) ⁱⁱ	O(4) ^{iv}		
O(1) ^{xi}	<i>1.831(9)</i>	3.251(3)	3.251(3)	3.251(3)			O(1) ^{xi}	<i>1.808(9)</i>	3.200(4)	3.200(4)	3.200(4)		
O(4)	109.3(2)	<i>2.148(3)</i>	3.510(2)	3.510(2)			O(4)	108.1(3)	<i>2.137(4)</i>	3.518(2)	3.518(2)		
O(4) ⁱⁱ	109.3(2)	109.6(2)	<i>2.148(3)</i>	3.510(2)			O(4) ⁱⁱ	108.1(3)	110.8(3)	<i>2.137(4)</i>	3.518(2)		
O(4) ^{iv}	109.3(2)	109.6(2)	109.6(2)	<i>2.148(3)</i>			O(4) ^{iv}	108.1(3)	110.8(3)	110.8(3)	<i>2.137(4)</i>		
Li(3)O₄ tetrahedron							Li(3)O₄ tetrahedron						
Li(3)	O(6) ^v	O(6) ^x	O(3) ^{xiii}	O(5) ^{viii}			Li(3)	O(6) ^v	O(6) ^x	O(3) ^{xiii}	O(5) ^{viii}		
O(6) ^v	<i>2.018(5)</i>	2.810(3)	3.966(3)	3.184(3)			O(6) ^v	<i>2.044(5)</i>	2.878(3)	3.976(3)	3.142(3)		
O(6) ^x	89.8(2)	<i>1.962(7)</i>	3.255(3)	3.332(2)			O(6) ^x	92.3(3)	<i>1.944(8)</i>	3.201(3)	3.293(3)		
O(3) ^{xiii}	157.8(3)	109.5(2)	<i>2.023(5)</i>	2.470(3)			O(3) ^{xiii}	155.6(4)	107.5(3)	<i>2.024(6)</i>	2.572(3)		
O(5) ^{viii}	105.7(2)	115.6(3)	76.3(2)	<i>1.975(5)</i>			O(5) ^{viii}	103.7(2)	115.5(3)	80.7(2)	<i>1.949(6)</i>		

Note. The Li–O distances are shown in italics. The O–Li–O angles are given below the diagonal and the distances O–O are given above.

Symmetry code: (ii) $1 - y, x - y, z$; (iv) $1 - x + y, 1 - x, z$; (v) $x, y, z - 1$; (vi) $-x, -y, 1 - z$; (vii) $-y, x - y, z - 1$; (viii) $y, y - x, 1 - z$; (ix) $y - x, -x, z - 1$; (x) $x - y, x, 1 - z$; (xi) $1 - y, 1 - x, 1/2 + z$; (xii) $1 - x + y, y, z - 1/2$.

As in the P_2O_7 unit, the shortest P–O distance involves the oxygen atom (O(1)) which is not bonded with a M atom and has a high thermal parameter.

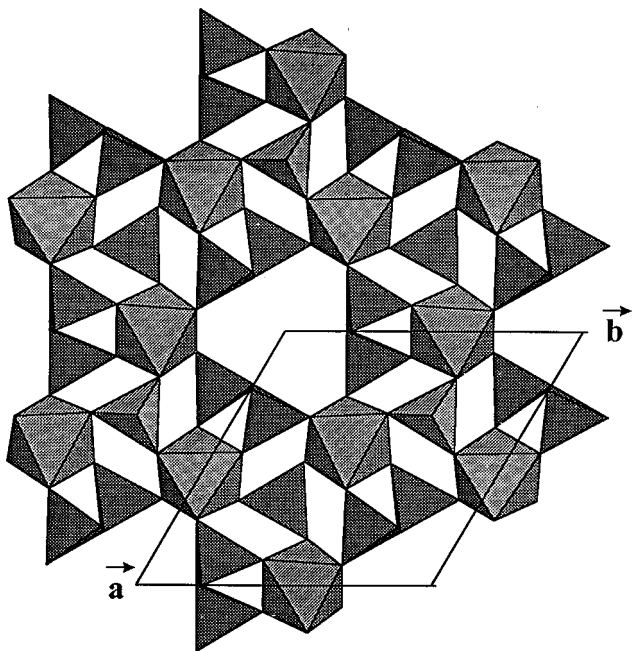


FIG. 1. Projection along [001] of an anionic layer $\infty[(\text{AlP}_2\text{O}_7)_3(\text{PO}_4)_2]^{9-}$ with $0.5 < z < 1$.

Cationic interlayers. The lithium ions are inserted between two anionic layers in three crystallographic sites (Fig. 3). Li(1) and Li(2) are located on the (2b) and (4d) special positions, respectively, while Li(3) is on a (12g) general position.

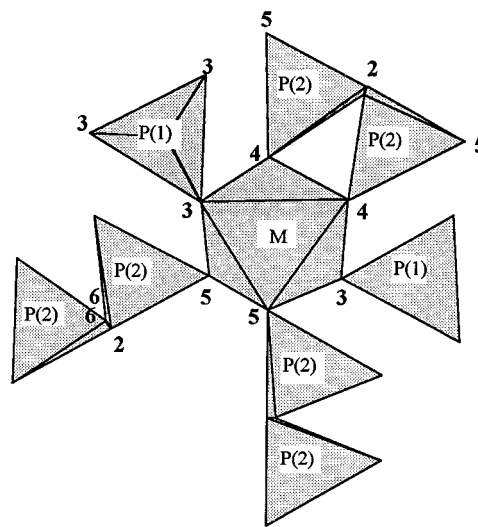


FIG. 2. Connection between the MO_6 octahedron and its neighboring PO_4 tetrahedra. Isolated numbers refer to oxygen atoms.

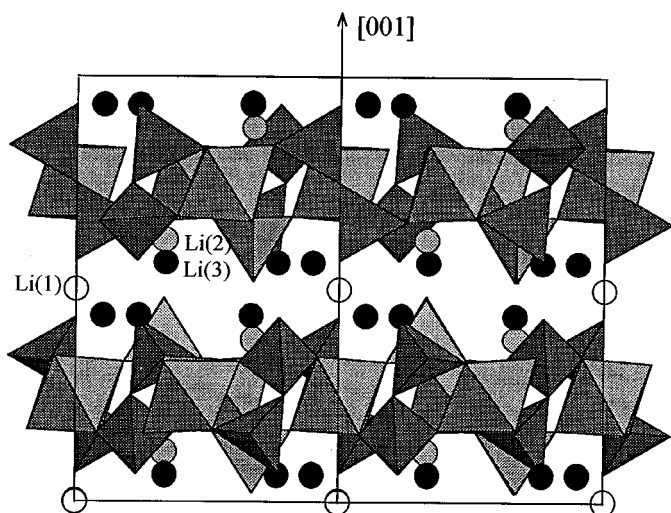


FIG. 3. Structure of $\text{Li}_9\text{Al}_3(\text{P}_2\text{O}_7)_3(\text{PO}_4)_2$: projection along $[110]$ showing the succession of anionic layers (polyhedra) and cationic inter-layers.

The stacking of anionic layers parallel to (001) results in tunnels running along c into which the Li(1) sites are located at $z = 0$ and $z = 1/2$ (Fig. 4). Li(1) lies at the center of a $\text{Li}(1)\text{O}(6)_6$ trigonal antiprism and exhibits a high Debye-Waller factor (Table 5). Li(2) is located on a ternary axis between two $\text{P}(1)\text{O}_4$ tetrahedra. It is tetrahedrally coordinated to one oxygen O(1) and three oxygens O(4) which lie at distances ranging from 1.81 to 2.15 Å. The next oxygen

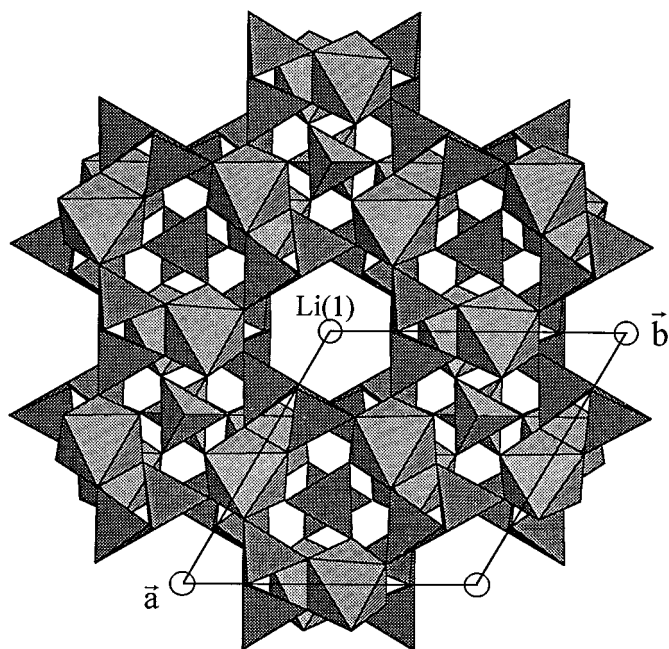


FIG. 4. Structure of $\text{Li}_9\text{Al}_3(\text{P}_2\text{O}_7)_3(\text{PO}_4)_2$: projection along c of two anionic layers.

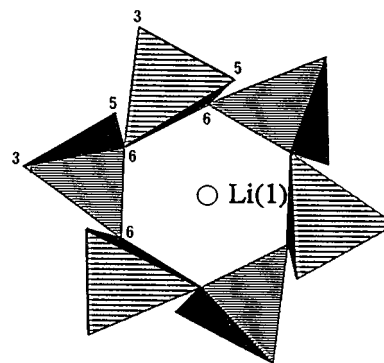


FIG. 5. Projection along $[001]$ of a Li_6O_{18} ring made up of six corner-sharing $\text{Li}(3)\text{O}_4$ tetrahedra (average $z = 0$). The Li(1) site (empty circle) occupies the center. Isolated numbers refer to oxygen atoms.

neighbors are three O(5) atoms at a distance of 2.91 ($M = \text{Al}$) or 3.00 Å ($M = \text{Fe}$). Li(3) is coordinated by a strongly distorted tetrahedron involving Li(3)–O distances ranging from 1.94 to 2.04 Å; a fifth oxygen neighbor (O(1)) lies at 2.859(4) ($M = \text{Al}$) or 2.945(4) Å ($M = \text{Fe}$). By sharing the oxygen atom O(6), six $\text{Li}(3)\text{O}_4$ tetrahedra form a $\text{Li}(3)_6\text{O}_{18}$ ring exhibiting a $\bar{3}$ internal symmetry and centered on Li(1) (Fig. 5). The $\text{Li}(1)\text{O}_6$ and $\text{Li}(3)\text{O}_4$ polyhedra share the O(6)–O(6) edges, while they have no oxygen atom in common with the $\text{Li}(2)\text{O}_4$ tetrahedron. The Li(2) and Li(3) ions display a rather low thermal agitation, slightly anisotropic, maximal in the vicinity of the (001) plane (Table 8).

CATION TRANSPORT PROPERTIES

Ionic Conductivity

Conductivity measurements were carried out in the temperature range 250 to 450°C on $\text{Li}_9M_3(\text{P}_2\text{O}_7)_3(\text{PO}_4)_2$ ($M = \text{Al}, \text{Fe}$) single crystals by the complex impedance method using a computer driven Hewlett-Packard 4192A impedance analyzer. The crystals selected for conductivity experiments were plates exhibiting surfaces parallel to (001) with area values ranging from 1 to 2 mm² and a thickness

TABLE 8
Root-Mean-Square Amplitudes of Anisotropic Displacement (Å) for Lithium in $\text{Li}_9M_3(\text{P}_2\text{O}_7)_3(\text{PO}_4)_2$ ($M = \text{Al}, \text{Fe}$)

	Atom	Minimum	Intermediate	Maximum
$M = \text{Al}$	Li(1)	0.225	0.225	0.239
	Li(2)	0.078	0.157	0.157
	Li(3)	0.103	0.115	0.149
$M = \text{Fe}$	Li(1)	0.203	0.297	0.297
	Li(2)	0.122	0.156	0.156
	Li(3)	0.112	0.135	0.161

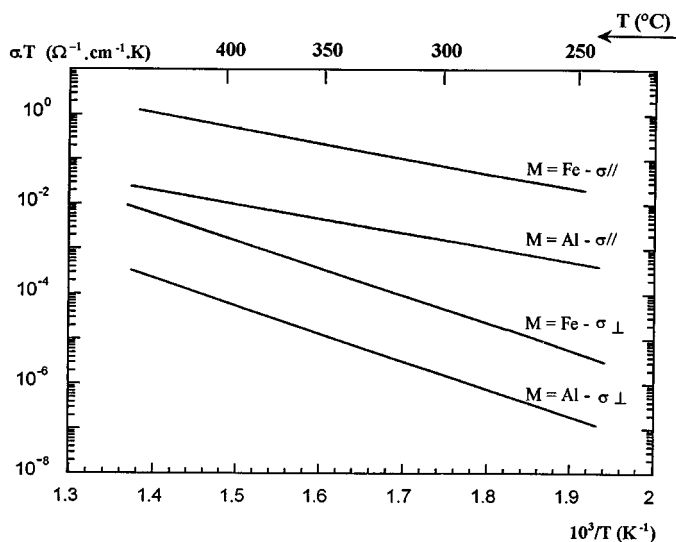


FIG. 6. Arrhenius plots of conductivity for single crystals $\text{Li}_9\text{M}_3(\text{P}_2\text{O}_7)_3(\text{PO}_4)_2$ ($M = \text{Al}, \text{Fe}$). $\sigma_{//}$ and σ_{\perp} refer to measurements made parallel and perpendicular to (001), respectively.

close to 0.2 mm in both cases. Appropriate faces were coated with silver or platinum paint in order to measure separately the conductivity parallel ($\sigma_{//}$) and perpendicular (σ_{\perp}) to (001). The results are presented in Fig. 6. Conductivity values at 300°C and conduction activation energies are listed in Table 10. For the sake of comparison, the corresponding values measured on a vitreous material having the same composition as the crystalline iron compound are also given.

Dc conductivity experiments using blocking electrodes were performed with a Keithley 487 picoammeter. They showed the electronic conductivity to be only a weak fraction of the total one ($\sigma_e/(\sigma_e + \sigma_i) < 1.5 \times 10^{-2}$).

TABLE 9
Radii of Oxygen Windows ($R_{\text{O-w}}$) for Lithium Coordination-Polyhedra of $\text{Li}_9\text{M}_3(\text{P}_2\text{O}_7)_3(\text{PO}_4)_2$

Cation	Window	$R_{\text{O-w}}$ (Å)	
		$M = \text{Al}$	$M = \text{Fe}$
Li(1)	O(6)–O(6)–O(6)	1.89	1.94
	O(6)–O(6)–O(6) ^a	2.17	2.23
Li(2)	O(1)–O(4)–O(4)	1.93	1.92
	O(4)–O(4)–O(4)	2.03	2.03
Li(3)	O(3)–O(6)–O(6) ^b	2.01	2.01
	O(3)–O(6)–O(5)	1.98	1.99
	O(3)–O(6)–O(5)	1.78	1.77
	O(5)–O(6)–O(6) ^c	1.81	1.80

^a Perpendicular to c .

^b For the Li(3) coordination polyhedron, the symbols O(3), O(5), O(6), and O(6)^c used in this Table correspond to O(3)^{xiii}, O(5)^{viii}, O(6)^v, and O(6)^x in Table 7.

TABLE 10
Conductivity σ ($\Omega^{-1}.\text{cm}^{-1}$) at 300°C and Conduction Activation Energy E_a (eV) in $\text{Li}_9\text{M}_3(\text{P}_2\text{O}_7)_3(\text{PO}_4)_2$ ($M = \text{Al}, \text{Fe}$) Single Crystals and in a Glass of Composition $\text{Li}_9\text{Fe}_3(\text{P}_2\text{O}_7)_3(\text{PO}_4)_2$

		$\sigma_{//}$	$E_{a//}$	σ_{\perp}	$E_{a\perp}$
Single crystals	$M = \text{Al}$	3.0×10^{-6}	0.66	3.5×10^{-9}	1.22
	$M = \text{Fe}$	1.3×10^{-4}	0.69	1.0×10^{-7}	1.20
Glass $\text{Li}_9\text{Fe}_3(\text{P}_2\text{O}_7)_3(\text{PO}_4)_2$		$\sigma = 2.4 \times 10^{-3}$. $E_a = 0.70$			

Ion Exchange

Exchange with molten salts. The cation exchange properties of $\text{Li}_9\text{Fe}_3(\text{P}_2\text{O}_7)_3(\text{PO}_4)_2$ were first investigated in molten nitrates ANO_3 ($A = \text{Na}, \text{Ag}$) used in a large excess ($A/\text{Li} > 5$), at a temperature of 355 and 295°C, respectively. In both cases, a partial exchange of Li^+ for A^+ took place with a progressive alteration of the crystal structure: after a 1-h treatment, the c parameter had increased, but new crystalline phases were also present. After four successive treatments in molten NaNO_3 , for a total duration of 18 h, only the Nasicon-type phase $\text{Na}_3\text{Fe}_2(\text{PO}_4)_3$ was present in the remaining solid.

Exchange with aqueous solutions. After a three-week treatment of a finely ground powder of $\text{Li}_9\text{Fe}_3(\text{P}_2\text{O}_7)_3(\text{PO}_4)_2$ by an aqueous solution of AgNO_3 ($\text{Ag}/\text{Li} = 5$) at room temperature, no exchange with Ag^+ was observed.

In contrast, in the presence of acidic solutions, a fast exchange reaction of Li^+ for H_{aq}^+ takes place. Simultaneously, the crystal undergoes a one-dimensional swelling in the c direction. The phenomenon is easily observable under the microscope by adding a droplet of concentrated HNO_3 to a suspension of tabular crystals of $\text{Li}_9\text{Fe}_3(\text{P}_2\text{O}_7)_3(\text{PO}_4)_2$: the tablet thickness increases rapidly up to several times its initial value and the crystal subdivides progressively into thin, optically uniaxial negative lamellae parallel to (001). The final solid resulting from reaction with a 1 M solution of HNO_3 ($\text{H}/\text{Li} = 10$) is X-ray amorphous. In order to avoid this amorphization and have a better understanding of the phenomenon, partial exchanges were performed using solutions of H_2SO_4 and LiNO_3 mixed in various ratios. These solutions are designated by S1, S2, S3 (Table 11). One millimole (0.94 g) of $\text{Li}_9\text{Fe}_3(\text{P}_2\text{O}_7)_3(\text{PO}_4)_2$ was immersed in 20 g of S1, S2, or S3. After 4 days, the solids were filtered, rapidly washed with water and propanone, air dried at room temperature, and then stored in atmospheres of various relative humidities. They were investigated by chemical, thermogravimetric (TG), and XRPD analyses. The results can be summarized as follows. (i) The solid resulting from the treatment with the most acidic solution, S3, was X-ray amorphous while those obtained using S1 and S2 were crystallized; their XRPD patterns recorded on samples

TABLE 11
Partial Exchange Reactions of Li^+ for H_{aq}^+ in $\text{Li}_9\text{Fe}_3(\text{P}_2\text{O}_7)_3(\text{PO}_4)_2$. Composition of the Solutions Used

Solution	Concentrations	
	LiNO_3	H_2SO_4
S1	5	0.315
S2	5	0.5
S3	5	1

Note. Concentrations are expressed in mol kg^{-1} .

contained in a humid atmosphere indicate the initial trigonal symmetry to be preserved with the a unit cell constant virtually unchanged but the c value strongly increased: $a = 9.778(5)$, $c = 18.27(2)$ Å for the S2-treated solid. (ii) The chemical and TG analyses of the samples show that a partial exchange reaction of Li^+ by H_{aq}^+ took place. As illustrated by Fig. 7, the extent of exchange increases from S1 to S3, i.e., with the acidity of the solution used. Simultaneously, the P/Fe ratio progressively decreases from its initial value 8 : 3, indicating some alteration of the anionic layer. Regardless of this alteration, we can represent the S2-treated material by the idealized formula $\text{Li}_{3.8}\text{H}_{5.2}\text{Fe}_3(\text{P}_2\text{O}_7)_3(\text{PO}_4)_2 \cdot n\text{H}_2\text{O}$, where n depends on the humidity h of the storage atmosphere: $n \approx 10, 7$ and 1 for $h = 80, 30$, and 3% , respectively. In the last case ($n \approx 1$) the c unit-cell constant is close to that measured for the initial, nonexchanged, anhydrous compound. Thus, the one-dimensional swelling observed during the ion-exchange reaction with acidic solutions appears to be associated with an uptake of water. Water molecules probably enter the cationic interlayer of the structure. Most of them can be reversibly removed by exposure of the solid to a dry atmosphere.

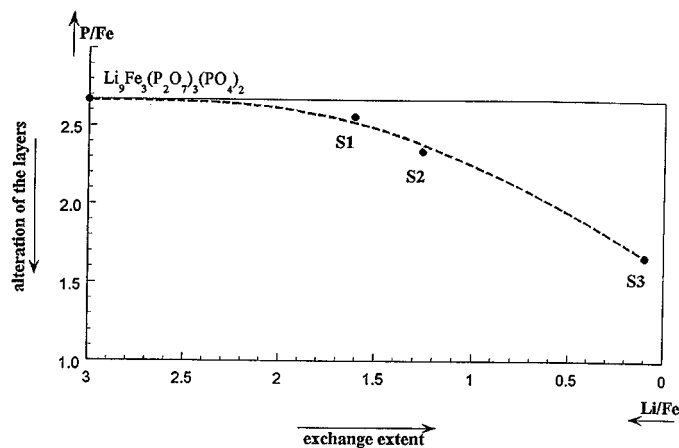


FIG. 7. Variation of the P/Fe molar ratio versus the Li/Fe molar ratio in solids resulting from a partial exchange of Li^+ for H_{aq}^+ in $\text{Li}_9\text{Fe}_3(\text{P}_2\text{O}_7)_3(\text{PO}_4)_2$.

DISCUSSION

The title compounds constitute a rare example of $\text{Li}-M^{\text{III}}$ phosphates having a layered structure (another case is probably the triphosphate $\text{Li}_2\text{MP}_3\text{O}_{10} \cdot 0-2\text{H}_2\text{O}$ obtained by ion exchange from $\text{H}_2\text{MP}_3\text{O}_{10} \cdot 2\text{H}_2\text{O}$ (30, 31)). Their cation transport properties appear relatively poor compared with those of several phosphates, characterized by a three-dimensional framework, such as $\text{Li}_3\text{M}_2(\text{PO}_4)_3$ -I, -II, and -III, $\text{Na}_3\text{M}_2(\text{PO}_4)_3$ (2) or $\text{Na}_7\text{M}_3(\text{P}_2\text{O}_7)_4$ (9, 10) which give fast ion-exchange reactions and have conductivities in the range $10^{-3}-2 \times 10^{-2} \Omega^{-1} \text{cm}^{-1}$ at 300°C .

However, the fast exchange of Li^+ by H_{aq}^+ exhibited by the new compounds with an insertion of water molecules between the layers and a one-dimensional expansion of the crystal is noteworthy and typical of layered ion exchangers. This two-dimensional character of the structure is also displayed by the single-crystal conductivity data, since the ratio $\sigma_{\parallel}/\sigma_{\perp}$ is about 10^3 for both crystals.

The conductivity values are higher for the iron than for the aluminum compound as observed in other compounds (32) but are relatively low in both cases. For $M = \text{Fe}$, they are even lower than the value measured for a glass of the same composition (14). Those rather low conductivities are consistent with the quasi-isotropic or slightly anisotropic character of the thermal motion of the lithium ions (Table 8).

No attempt was made to determine the possible diffusion paths for Li^+ ions inside the cationic interlayer; since two neighboring anionic layers are connected by lithium ions, the diffusion of these ions might strongly modify, locally and temporarily, the radii of the oxygen windows ($R_{\text{O-w}}$) along the paths. As a consequence, the $R_{\text{O-w}}$ values calculated from the coordinates of the oxygen atoms are probably of little significance. Nevertheless, we can notice that most of the triangular windows formed by the faces of the lithium coordination polyhedra (Table 9) may be considered as possible passageways for the Li^+ ions, since their radius is higher than (or close to) the sum Σ of the ionic radii (33), $r(\text{Li}^+) + r(\text{O}^{2-}) \approx 1.94$ Å.

Another problem is posed by the low conductivity observed along c . The $\text{Li}(1)$ ion resides into a tunnel parallel to $[001]$. Two neighboring lithium ions in the tunnel are located at a distance of $c/2 \approx 6.8$ Å; they are separated by two equilateral triangle-shaped windows delimited by oxygen atoms $\text{O}(2)$. The radii $R_{\text{O-w}}$ of these windows are equal to 1.98 and 2.07 Å for the aluminum and the iron compounds, respectively. Thus, in both cases, they satisfy the relation $R_{\text{O-w}} > \Sigma$. On the basis of this geometrical criterion, a fast conduction by lithium ions could be expected in the $[001]$ direction; but it is not confirmed by the conductivity measurements. Although ionic conduction in solids is a much too complex phenomenon to be simply interpreted, a qualitative explanation is suggested by the

two following facts. (i) The aluminum compound, for which R_{O-w} is smaller, exhibits a lower conductivity along c than the iron member (Table 10 and Fig. 6); that seems to indicate an important role played by some geometrical factors. (ii) The oxygen atoms O(2), which form windows in the tunnel, are bridging oxygens of the diphosphate units. It is well known (28) that in condensed phosphates, such oxygen atoms contribute rarely to the near environment of the cations; when they do, their distance from the cation is always higher than the shortest cation–oxygen distance of the coordination polyhedron. (In a simple electrostatic approach, these observations could be interpreted as a weaker attraction of the cation by a bridging-oxygen than by a terminal one, due to the less negative charge carried by the first.) Therefore, the relation $R_{O-w} \geq \Sigma$ usually considered as a condition for a fast ion diffusion in solids would be replaced by $R_{O-w} \geq \Sigma'$ with $\Sigma' > \Sigma$. In the crystals under study, the tunnels perpendicular to the layer would not be wide enough to allow a fast lithium conduction along c .

REFERENCES

1. M. Pintard-Scrépel, F. d'Yvoire, and F. Rémy, *C.R. Acad. Sci. Paris Sér. C* **286**, 381 (1978).
2. F. d'Yvoire, M. Pintard-Scrépel, E. Bretey, and M. de la Rochère, *Solid State Ionics* **9/10**, 851 (1983).
3. C. Delmas, J.-C. Viala, R. Olazcuaga, G. Le Flem, and P. Hagenmuller, *Solid State Ionics* **3/4**, 209 (1981).
4. I. S. Lyubutin, O. K. Melnikov, S. E. Sigaryov, and V. G. Terziev, *Solid State Ionics* **31**, 197 (1988).
5. A. B. Bykov, A. P. Chirkin, L. N. Demyanets, S. N. Doronin, E. A. Genkina, A. K. Ivanov-Shits, I. P. Kondratyuk, B. A. Maksimov, O. K. Mel'nikov, L. N. Muradyan, V. I. Simonov, and V. A. Timofeeva, *Solid State Ionics* **38**, 31 (1990).
6. C. Masquelier, A. K. Padhi, K. S. Nanjundaswamy, S. Okada, and J. B. Goodenough, in "Proceedings of the 37th Power Sources Conference," Hilton at Cherry Hill, New Jersey, p. 188, June 1996.
7. A. K. Ivanov-Shits and J. Schoonman, *Solid State Ionics* **91**, 93 (1996).
8. M. de la Rochère, A. Kahn, F. d'Yvoire, and E. Bretey, *Mater. Res. Bull.* **20**, 27 (1985).
9. C. Masquelier, F. d'Yvoire, and N. Rodier, *J. Solid State Chem.* **95**, 156 (1991).
10. C. Masquelier, F. d'Yvoire, E. Bretey, P. Berthet, and C. Peytourt-Chansac, *Solid State Ionics* **67**, 183 (1994).
11. P. Berthet, E. Bretey, J. Berthon, F. d'Yvoire, A. Belkebir, A. Rulmont, and B. Gilbert, *Solid State Ionics* **70/71**, 476 (1994).
12. T. Tsuchiya and N. Yoshimura, *J. Mater. Sci.* **24**, 493 (1989).
13. K. C. Sobha and K. J. Rao, *Solid State Ionics* **81**, 145 (1995).
14. S. Poisson, Thèse de Doctorat, Université Paris-Sud, Orsay, France, 1997.
15. F. Rémy, *Bull. Soc. Chim. Fr.* 3380 (1969).
16. B. Wunderlich, *Acta Crystallogr. B* **35**, 265 (1979).
17. J. C. Guitel and I. Tordjman, *Acta Crystallogr. B* **32**, 2960 (1976).
18. J. R. Van Wazer, "Phosphorus and Its Compounds," Vol. 1. Interscience, New York, 1958.
19. F. d'Yvoire, *Bull. Soc. Chim.* 1237 (1962).
20. C. K. Fair, "An Interactive Intelligence System Crystal Structure Analysis," Delft, 1990.
21. P. Coppens, L. Leiserowitz, and D. Rabinovich, *Acta Crystallogr.* **18**, 1035 (1965).
22. M. C. Burla, M. Camalli, G. Cascarano, C. Giacovazzo, G. Polidori, R. Spagna, and D. Viterbo, *J. Appl. Cryst.* **22**, 389 (1989).
23. D. Riou, N. Nguyen, R. Benloucif, and B. Raveau, *Mater. Res. Bull.* **25**, 1363 (1990).
24. M. Gabelica-Robert, M. Goreaud, Ph. Labbé, and B. Raveau, *J. Solid State Chem.* **45**, 389 (1982).
25. Hok Nam Ng and C. Calvo, *Can. J. Chem.* **51**, 2613 (1973).
26. D. Riou, Ph. Labbé, and M. Goreaud, *Eur. J. Solid State Inorg. Chem.* **25**, 215 (1988).
27. C. Masquelier, F. d'Yvoire, and N. Rodier, *Acta Crystallogr. C* **46**, 1584 (1990).
28. A. Durif, "Crystal Chemistry of Condensed Phosphates." Plenum Press, New York, 1995.
29. F. d'Yvoire, E. Bretey, and G. Collin, *Solid State Ionics* **28/30**, 1259 (1988).
30. F. d'Yvoire, *Bull. Soc. Chim. France* 1224 (1962).
31. P. Rémy and A. Boullé, *Bull. Soc. Chim. France* 1838 (1968).
32. C. Masquelier, F. d'Yvoire, and G. Collin, *J. Solid State Chem.* **118**, 33 (1995).
33. R. D. Shannon, *Acta Crystallogr. A* **32**, 751 (1976).